changes the nature but not the position of the leading singularity.

VI. CONCLUSIONS

(1) We have seen that the exact sum of bubble graphs in the massless ϕ^4 theory has analytic properties in the n plane distinct from the potential theory situation where the Fredholm theory is applicable.[4]

(2) The weak-coupling limit of our result agrees with Sawyer's result for massless pions obtained by summing the most singular terms of perturbation theory. Comparison with Sawyer's result for massive pions shows that neglect of the pion mass does not alter the position of the leading singularity (at least in the weak-coupling limit).

(3) Our third motive which was to reduce a more general problem to a Fredholm equation has been only partially carried out. What remains to be done is to solve Eq. (III.2) with $\mu \neq 0$.

(4) The method of Bjorken seems to be a very useful technique for solving the forward scattering problem. The resulting equations are much simpler than the usual partial-wave equations.

ACKNOWLEDGMENTS

We are deeply indebted to Dr. James Bjorken whose lectures at the University of Washington provided the basis for this work, and to Dr. R. Sawyer for invaluable discussions. One of the authors (M.B.) is grateful to the Sloan Foundation Grant for support.

PHYSICAL REVIEW VOLUME 132, NUMBER 5 1 DECEMBER 1963

Meson Production in $p+d$ Collisions and the $I=0$ π-π Interaction. I. Measured Momentum Spectra of He^3 and H^3 Nuclei from High-Energy $p+d$ Collisions*

ALEXANDER ABASHIAN,† NORMAN E. BOOTH,‡ KENNETH M. CROWE, ROGER E. HILL,‡ AND ERNEST H. ROGERS§
Lawrence Radiation Laboratory, University of California, Berkeley, California

(Received 17 June 1963)

The momentum spectra of He^3 and H^3 nuclei produced in $p+d$ collisions have been measured with high resolution. Data were obtained at several angles and incident proton energies of about 745 MeV. Each spectrum exhibits a peak due to single pion production and a continuum due to double pion production. An anomalous bump has been observed in the He^3 spectra which we interpret as an $I=0$ virtual di-pion with a scattering length of $2\hbar/\mu c$. In this series of four papers we summarize the data obtained over a series of three cyclotron runs. The first paper deals with the experiment and techniques, and the second with the results of the measurements on single-pion production. Next we describe an experiment to determine the spin and parity of the anomalous bump, and finally we discuss its interpretation.

I. INTRODUCTION

IT is widely known that in a nuclear or elementary-particle interaction, if one measures the energy spectrum of one type of outgoing particle, information about the nature of the remainder of the outgoing particles can be obtained. In particular, there is a unique (although sometimes double-valued) correspondence between the vector momentum of one of the particles and the total energy in the rest system of the remaining particles. Any stable or resonant value of this total energy is reflected as a bump in the spectrum of the first particle. Referring to the inset of Fig. 1, consider a particle of momentum $\mathbf{p}_1$ striking particle 2 and yielding a particle of momentum $\mathbf{p}_3$ and a group of one or more particles whose momenta add up to $\mathbf{p}_w$. Energy and momentum conservation gives $\mathbf{p}_w=\mathbf{p}_1-\mathbf{p}_3$ and $E_w=E_1+m_2-E_3=(|\mathbf{p}_w|^2+w^2)^{1/2}$, where w is the "mass" or total energy in the rest system defined

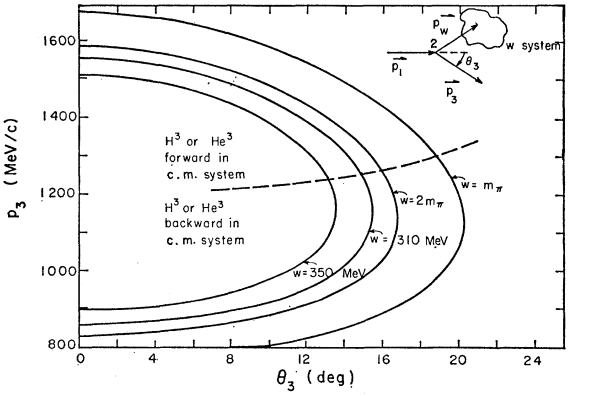

FIG. 1. Kinematical plots of H^3 and He^3 momentum from $p+d$ collisions with 740-MeV protons. The curves are plotted versus the laboratory angle of the H^3 or He^3 for various values of w, the "mass" of the system produced with the H^3 or He^3.

* This work was done under the auspices of the U. S. Atomic Energy Commission.

† Present address: Physics Department, University of Illinois, Urbana, Illinois.
‡ Present address: Enrico Fermi Institute for Nuclear Studies, University of Chicago, Chicago, Illinois.
§ Present address: Aerospace Corporation, El Segundo, California.

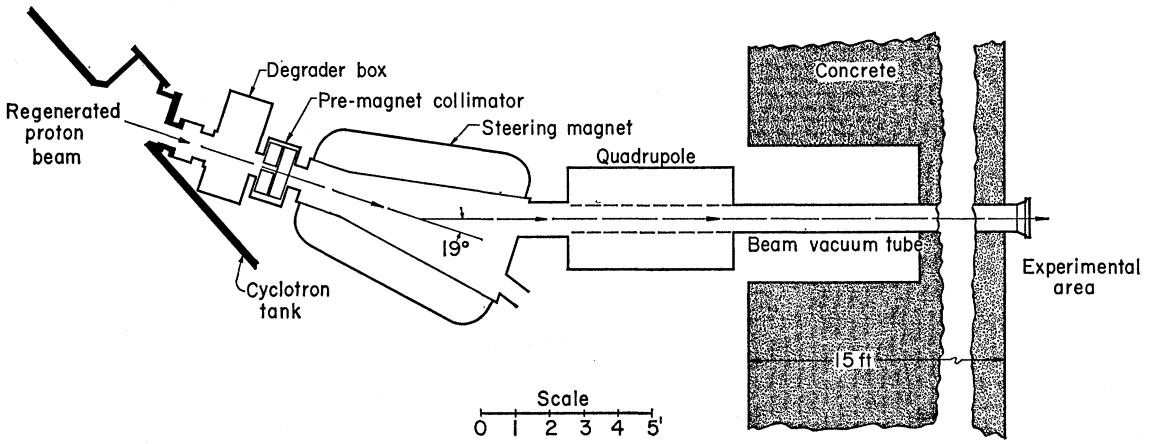

FIG. 2. Layout of the regenerated proton beam of the 184-in. synchrocyclotron.

by $\mathbf{p}_w'=0$. Thus, measuring $\mathbf{p}_3$ gives w according to $w^2=(E_1+m_2-E_3)^2-(\mathbf{p}_1-\mathbf{p}_3)^2$. If the "$w$ system" consists of, say, two pions of mass μ and momenta $\mathbf{p}_4$ and $\mathbf{p}_5$, then $\mathbf{p}_w=\mathbf{p}_4+\mathbf{p}_5$, and w is the total energy in the center-of-mass (c.m.) system of the two pions. If we let $\mathbf{p}_4'=-\mathbf{p}_5'=\mathbf{q}$, then we have $w=2(q^2+\mu^2)^{1/2}$.

In the series of experiments described in this paper, deuterons were bombarded with protons, and the measured or "spectator" particle was a He^3 or H^3 nucleus. Since there are no remaining nucleons, the w system consists only of one or more pions. Thus, in the energy spectrum of H^3 or He^3, we expect to find peaks due to the reactions

$$p+d\rightarrow He^3+\pi^0 \quad (1a)$$
$$\rightarrow H^3+\pi^+ \quad (1b)$$

and continua due to the reactions

$$p+d\rightarrow He^3+\pi^0+\pi^0 \quad (2a)$$
$$\rightarrow He^3+\pi^+\pi^- \quad (2b)$$
$$\rightarrow H^3+\pi^+\pi^0. \quad (2c)$$

This is made clearer by reference to the curves of Fig. 1.

It is appropriate at this point to summarize the results of isotopic-spin considerations for these reactions. For reactions (1) the pertinent isospin function is

$$\psi_{1/2}{}^{1/2}=(2/3)^{1/2}\,H^3\pi^+-(1/3)^{1/2}\,He^3\pi^0,$$

where the subscript is the total isospin, and the superscript is its z component. Thus we have

$$\frac{\sigma(p+d\rightarrow H^3+\pi^+)}{\sigma(p+d\rightarrow He^3+\pi^0)}=2.$$

For double-pion (2π) production we label the isospin functions according to the isotopic spin of the two pions and write

$$\psi_{1/2}{}^{1/2}(I=1)=(2/3)^{1/2}\,H^3\Pi_1{}^1-(1/3)^{1/2}\,He^3\Pi_1{}^0$$

and

$$\psi_{1/2}{}^{1/2}(I=0)=He^3\Pi_0{}^0,$$

where

$$\Pi_1{}^1=(1/2)^{1/2}(\pi^+\pi^0-\pi^0\pi^+),$$
$$\Pi_1{}^0=(1/2)^{1/2}(\pi^+\pi^--\pi^-\pi^+),$$
$$\Pi_0{}^0=(1/3)^{1/2}(\pi^+\pi^-+\pi^-\pi^+-\pi^0\pi^0).$$

Then, if $\sigma_{I=0}$ and $\sigma_{I=1}$ represent cross sections for definite isotopic spin $I=0$, 1 for the two pions, we have the relations

$$\sigma_{I=0}(He^3\pi^+\pi^-)=2\sigma_{I=0}(He^3\pi^0\pi^0),$$
$$\sigma_{I=1}(H^3\pi^+\pi^0)=2\sigma_{I=1}(He^3\pi^+\pi^-),$$
$$\sigma_{I=0}(H^3\pi^+\pi^0)=\sigma_{I=1}(He^3\pi^0\pi^0)=0.$$

We now describe the technical details of the experiments and shall return to the analysis in papers II and IV.

II. PROTON BEAM

The proton beam was obtained by regenerative extraction from the Berkeley 184-in. synchrocyclotron under somewhat different conditions for the three runs. After emerging from the cyclotron the beam passes through a box into which a degrader can be inserted to lower the proton energy. Next (see Fig. 2) there are two sets (vertical and horizontal) of collimating slits which can be adjusted in aperture and position. We refer to these slits as the premagnet collimator (PMC). A steering magnet then bends the beam through 19 deg into a quadrupole lens system which focuses the beam in the experimental area. Approximately 15 ft of concrete separate the experimental area from the focusing and steering magnets.

Beam size and position can be checked in the experimental area with x ray or Polaroid film or with a television camera that looks at a 1-in.-thick piece of plastic scintillator. With the PMC wide open (i.e., 4 by 4 in.) and with optimum focusing conditions, the most intense part of the beam is contained in a 1-in.-diam circle, and more than 90% of the beam in a

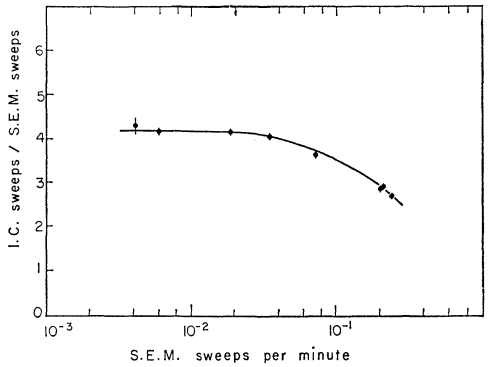

FIG. 3. Measurement of ion-chamber saturation, and calibration of the secondary-emission monitor (SEM). Each SEM sweep corresponds to 4.2×10^{12} protons. The flat part of the curve gives 0.47 for the multiplication factor of SEM.

3-in.-diam circle. The beam energy is not too well determined because the energy spectrum is rather broad.[1] However, by using the PMC, one can separate out a fairly monoenergetic part of the beam which can be brought to a focus of $\approx 1/2$ in. in diameter. The intensity of this beam is about one-fifth of the total extracted beam.

We used the following procedure to obtain a monoenergetic well-focused beam. With the television camera in position viewing the plastic scintillator, we mapped out the beam by using a 1/2- by 1/2-in. aperature in the PMC and moving it about. It was found that for a range of positions of the PMC a small, fairly intense beam spot was obtained, while for others a second spot or diffuse area with a larger energy spread appeared. We chose a position and aperture for the PMC such that a small monoenergetic beam spot was obtained with maximum intensity. Taking into account the optics of the beam and the momentum analysis of the steering magnet, we calculated that the maximum beam energy spread was about 20 MeV, and could be much smaller.

For the first run the focusing quadrupole was a 4-in.-diam triplet. The optics and beam intensity were improved for the second and third runs by replacing the triplet with an 8-in.-aperture doublet. The intensity of the selected beam was typically 4×10^{10} protons per sec.

Under normal operating conditions the beam emerged 64 times a second in 200-μsec bursts, upon which the 20-Mc/sec radiofrequency structure is superimposed. Toward the end of the second run an auxilliary dee was installed in the cyclotron which allowed the 200-μsec bursts to be stretched to 8 to 10 msec. This improvement in duty cycle minimized accidental problems and allowed us to perform the coincidence experiment discussed in paper III.

As monitors of beam intensity, we used an argon-filled ionization chamber and a secondary-emission monitor (SEM).[2] The multiplication factor of the ion chamber can be computed from the value of dE/dx in argon and has been checked with 345-MeV protons.[3] The ion chamber saturates at high beam intensities, whereas the SEM remains linear. The multiplication factor of the SEM was obtained by measuring the ratio of ion-chamber current to the SEM current at low beam intensities; a typical calibration curve is shown in Fig. 3. The linearity of SEM was checked at the higher beam intensities by means of a second ion chamber placed near but not in the main beam.

One method of determining the proton beam energy is to find its range in copper from a Bragg curve. Figure 4 shows the last part of a Bragg curve obtained by placing two ion chambers in the proton beam with copper between them and measuring the ratio of their currents as the thickness of copper is varied. An analysis of this curve from data taken in the first run using the method of Mather and Segrè[4] and the range-energy tables of Rich and Madey[5] gives 740 ± 3 MeV for the proton energy. We found it more consistent, though not necessarily more accurate, to determine the proton energy from our experimental momentum spectra. Particle momentum in terms of the currents in our spectrometer magnets was determined by the current-carrying wire method to better than 0.5%. Measurement of the momentum of the He^3 peak from the reaction $p+d\rightarrow He^3+\pi^0$, corrected for energy loss of the He^3 between the target center and our momentum-analysis system, allowed us to compute the proton energy from kinematics. The only other parameter is

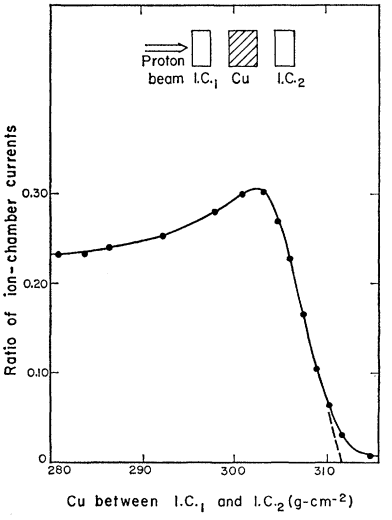

FIG. 4. Last part of Bragg curve of the incident proton beam. The curve gives a mean range of 306.6 g/cm^2 of Cu. Adding 1.9 g/cm^2 due to other materials in the beam gives $T_p=740$ MeV.

[1] S. von Friesen and W. H. Barkas, Lawrence Radiation Laboratory Note UCID-613, January 1959 (unpublished).

[2] G. W. Tautfest and H. R. Fechter, Rev. Sci. Instr. **26**, 229 (1955).

[3] O. Chamberlain, E. Segrè, and C. Wiegand, Phys. Rev. **82**, 923 (1951).

[4] R. Mather and E. Segrè, Phys. Rev. **84**, 191 (1951).

[5] M. Rich and R. Madey, Lawrence Radiation Laboratory Report UCRL-2301, 1954 (unpublished).

the scattering angle, which was measured to ± 0.05 deg with x-ray film and a transit.

III. DEUTERIUM TARGET

By using a well-defined proton beam and a gaseous target, we can arrange collimating slits for a scattered beam such that particles scattered from the walls and windows of the gas container cannot get through the slits. To obtain the small deuterium thickness necessary for good momentum resolution with liquid deuterium; we would have to have the walls of the liquid container comparable in thickness to the deuterium. This would result in a large background from interactions in the walls of the liquid container. With a gaseous target, we achieved backgrounds of typically 1 or 2%.

Although somewhat different targets were used in the three runs, we describe here only the target used in the third run. It was designed for angles between 13 and 17 deg to the incident beam direction and is shown in Fig. 5 set up for a scattering angle of 13.5 deg. The exit windows for the proton and scattered beams were 1-in.-diam, 0.010-in.-thick Al. As can be seen from Fig. 5, the entrance and exit windows for the proton beam cannot be "seen" by the slit system. The target was tested at pressures of up to 750 psi and was normally operated at ~ 300 psi corresponding to a D_2

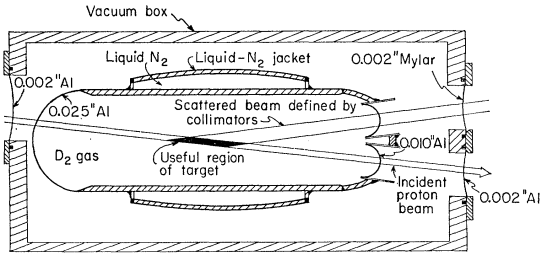

FIG. 5. High-pressure D_2 gas target used in the third run.

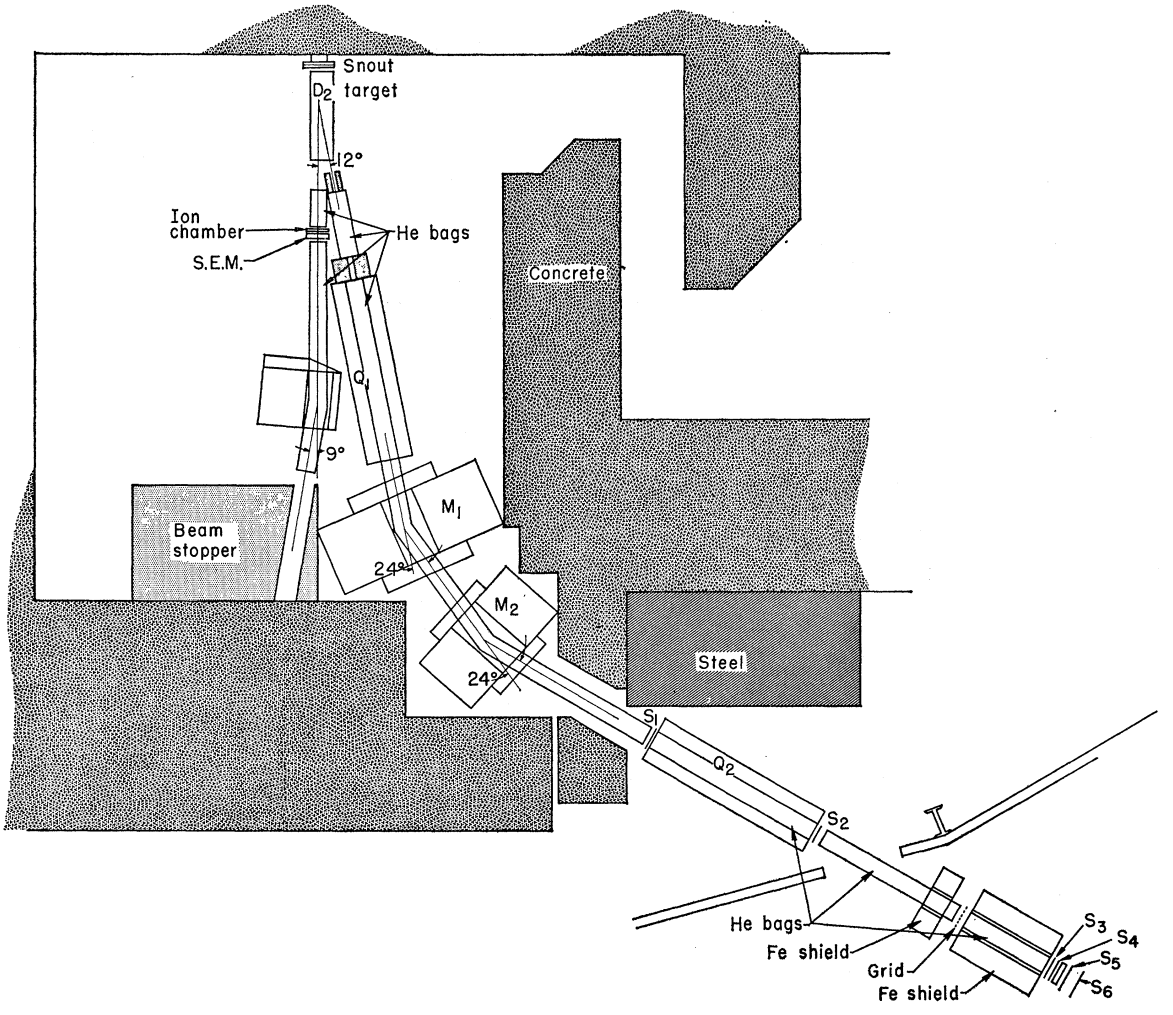

FIG. 6. Experimental arrangement used in the second run.

TABLE I. Details of collimating slits for momentum-selected beams.

Run	First slit (in.) Hor.	Vert.	Second slit (in.) Hor.	Vert.	Slit separation (in.)	rms $\delta\theta$ (deg)	$\Delta\Omega$ (sr)
1	0.27	1.0	0.53	3.0	41	0.17	1.1×10^{-4}
2	0.5	1.0	0.5	3.0	50	0.19	1.2×10^{-4}
3	0.5	1.0	0.5	2.75	46	0.20	2.1×10^{-4}

density of about 15 g/liter. The target was filled with a compressor from a large surge tank, and was emptied back into the surge tank. Backgrounds were taken by pumping out the residual deuterium after emptying, and introducing hydrogen gas at the same pressure. This gave the same stopping power to He^3 and allowed us to check that He^3 nuclei were not being produced spuriously, for example, by protons interacting with the collimating slits. The density of the gas in the target was determined from a calibrated pressure gauge and thermocouples soldered at various points on the target. Conditions were reproducible from day to day if at least an hour was allowed for the target to come to thermal equilibrium after filling.

IV. COLLIMATING SLITS

The collimating slits were of brass, 12 in. long, sometimes with tungsten inserts. Apart from the considerations of the previous section, their apertures were designed to ensure that the solid angle was defined by the slits and not by any part of the spectrometer system, and to optimize the momentum resolution. Table I gives details of the slit apertures used.

V. MOMENTUM ANALYSIS

The magnetic spectrometer systems used in the first two runs have been described briefly before.[6,7] The systems were only slightly different, and we give here details pertaining mainly to the second and third runs. The spectrometer was designed to optimize the momentum resolution, keeping in mind the geometrical limitations due to walls and other obstructions of the cyclotron building, and to have a long enough path for the time-of-flight measurements.

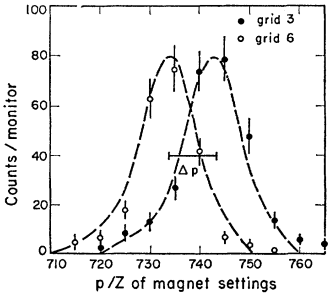

FIG. 7. Magnetic sweep of He^3 from $p+d \rightarrow He^3+\pi^0$ as measured in two different grid counters to determine the momentum acceptance.

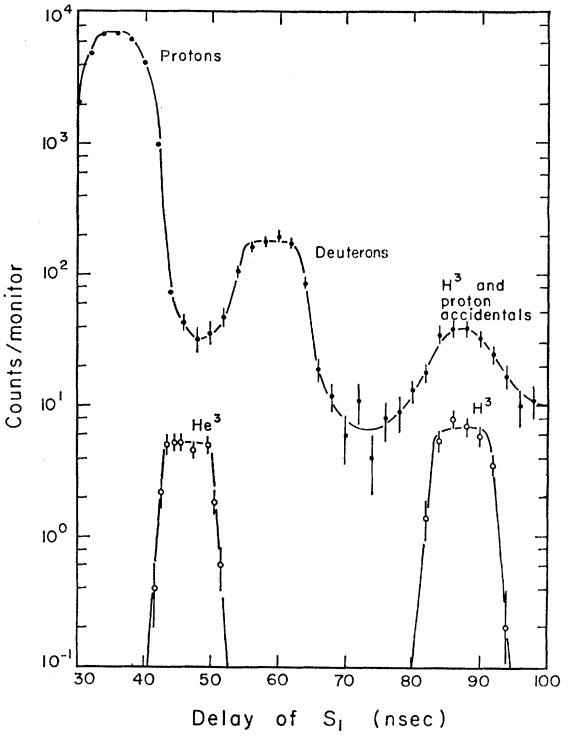

FIG. 8. Typical time-of-flight curves. Solid circles show the result of varying the delay of S_1 with respect to S_3 and S_4. The open circles are obtained when dE/dx and range requirements are satisfied.

For the first experiment which was designed to measure only He^3 momentum spectra, the spectrometer setup was similar to that shown in Fig. 6 except that the scattered beam was brought to a focus between the two bending magnets M_1 and M_2. A collimating slit here defined the "momentum acceptance" $\Delta p/p$. The beam was then refocused by quadrupole Q_2 onto the counters at the end of the system.

In the second and third runs, where we wanted to measure H^3 spectra also, it was necessary to decrease the angles of bend of M_1 and M_2 and to focus only at the end of the system. However this had the advantage that we could define the "momentum acceptance" by the width of a counter at the focus, and by using a grid

TABLE II. Magnet systems.

Run	Angle of bend (deg) M_1	M_2	$\Delta p/p$ (%)
1	41	35	1.2[a]
2	24	24	0.45 per grid
3	25	25	0.38 per grid

[a] For data taken at reduced proton energies, $\Delta p/p = 4.9\%$.

[6] A. Abashian, N. E. Booth, and K. M. Crowe, Phys. Rev. Letters 5, 258 (1960).
[7] N. E. Booth, A. Abashian, and K. M. Crowe, Phys. Rev. Letters 7, 35 (1961).

of several counters, take several data points simultaneously. In the third run an additional H-type magnet was placed before the target, which permitted us to change the scattering angle by changing the angle of the proton beam, keeping the target and spectrometer fixed. The H-magnet was mounted so that it could be easily rotated and translated. The correct positions and currents were determined by x-ray pictures of the proton beam.

The spectrometer used in the second and third runs was a symmetrical system consisting of a triplet quadrupole Q_1 which focused the produced particles at infinity, two bending magnets, M_1 and M_2, for momentum analysis and a second quadrupole Q_2 which refocused the analyzed beam at the positions of the grid counters G_1 through G_8. There was some chromatic aberration at G_1 through G_8, but this was not sufficient to require positioning each grid at a slightly different distance from Q_2. By means of ray tracing we could determine the proper collimation to ensure the transmission of all particles of a chosen momentum. The currents in the bending magnets were determined for several momenta by passing a current-carrying wire through the entire system. The measurements were reproducible to better than 0.5%. The currents for the quadrupoles were determined by computer calculations and checked by passing the current-carrying wire through one of the quadrupoles and the adjacent bending magnet. All magnet currents were regulated to about 0.1%.

The momentum acceptance, or width of each grid in terms of momentum ($\Delta p/p$), was obtained by taking a series of counts in each grid as the He^3 peak from the reaction $p+d \rightarrow He^3+\pi^0$ was swept across the grids. An example is shown in Fig. 7. Table II gives details of the magnet systems.

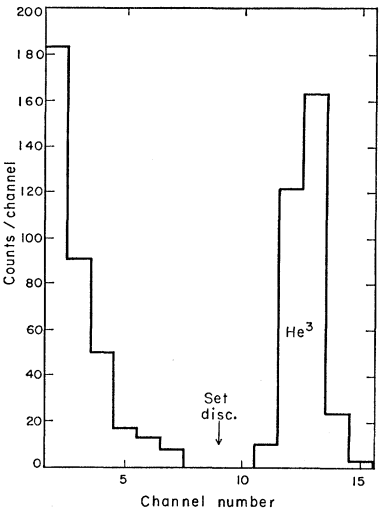

FIG. 9. Pulse-height spectrum in S_3 for He^3 at $p/z = 680$ MeV/c.

VI. COUNTERS AND ELECTRONICS

The momentum-selected secondary beam consisted mainly of protons and deuterons. From these it was necessary to separate out the He^3 and H^3 of interest. Time-of-flight was the first electronic requirement and was measured between counter 1 and counters 3 and 4, a flight path of about 15 ft. A typical timing curve is shown in Fig. 8. In order to reject a large fraction of the protons, a range requirement was made by

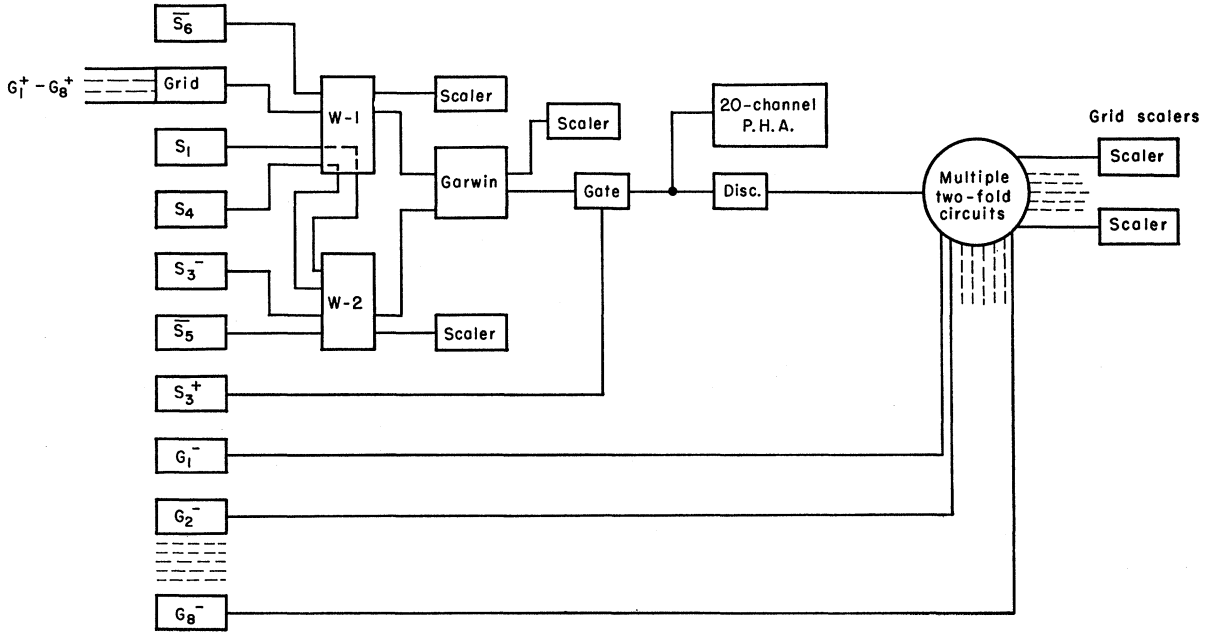

FIG. 10. Block diagram of the electronics.

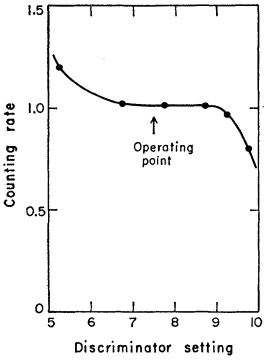

FIG. 11. Tunnel-diode discriminator curve for one of the counters in the third run.

placing sufficient Cu to stop He^3 or H^3 in front of counters 5 and 6 and placing them in anticoincidence. Additional rejection was obtained by pulse-height analysis of the energy loss in S_3. The lower curves of Fig. 8 are the results obtained with the range and dE/dx requirements. A typical pulse-height spectrum for He^3 is shown in Fig. 9. The spectrum was obtained by gating a 20-channel pulse-height analyzer with the coincidence $S_1S_3S_4\bar{S}_5\bar{S}_6$ and displaying the pulse from S_3. There is good separation between He^3 and the smaller pulses that are due mainly to protons. Details of the electronic arrangement are shown in Fig. 10.

Timing curves were taken at three or four different momenta and then interpolated to find the correct delays at any other momentum. After the He^3 or H^3 delay for S_1 had been determined, grid counters G_1 through G_8 were switched into coincidence and delayed with a slightly larger resolving time. For the H^3 measurements, another counter S_{12} was placed in the time-of-flight path to obtain better rejection against proton accidentals. This was particularly necessary at momenta near 1350 MeV/c, which corresponds to nucleon-nucleon scattering in deuterium. The discriminator shown in Fig. 10 in parallel with the pulse-height analyzer was set to count only the particles of interest, for instance, at a level corresponding to channel 9 in Fig. 9. Then the multiple twofold circuits opened only when a particle of the desired type passed through one of the grid counters, and we were able to read off the distribution of counts in the grids directly from the grid scalers. The total of these grid counts always agreed well with the H^3 or He^3 peaks in the pulse-height analyzer.

Coincidence counters were $\frac{1}{16}$-in.-thick plastic scintillator, except the dE/dx counter S_3 which was $\frac{1}{4}$-in.-thick. In the third run a thinner S_1, 0.015 by 8 in. in diameter, was used to reduce multiple scattering and improve momentum resolution. Also the counters were designed to be more uniform across their area in pulse height. Although this resulted in poorer timing because of fewer photoelectrons, we required that the pulses in three of the counters be above a certain level. This multiplicative rejection of smaller pulses due to protons and deuterons made the separation somewhat cleaner even with the poorer timing and was made

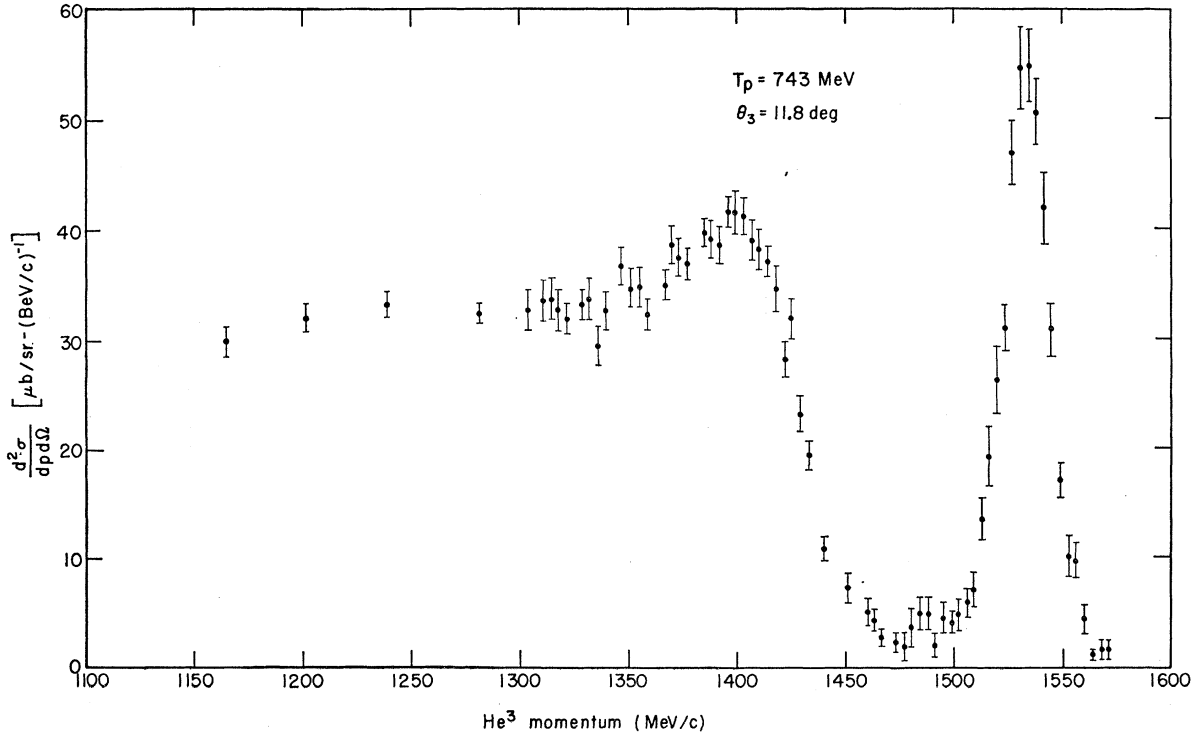

FIG. 12. Measured He^3 momentum spectrum for $\theta = 11.8$ deg.

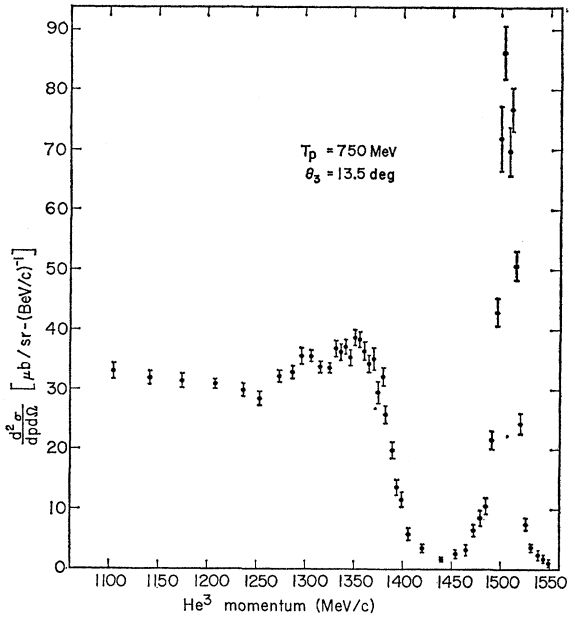

FIG. 13. Measured He^3 momentum spectrum for $\theta=13.5$ deg.

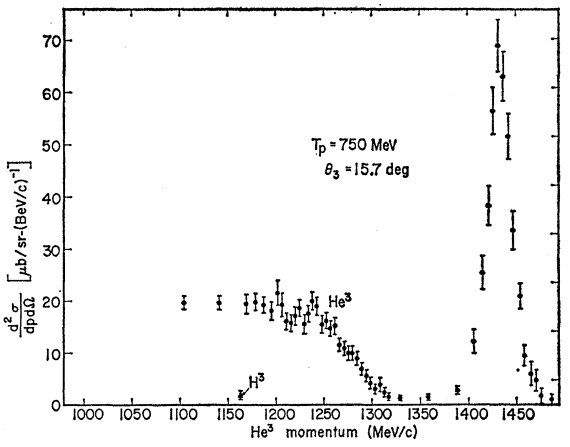

FIG. 14. Measured He^3 momentum spectrum and a single H^3 measurement for $\theta=15.7$ deg.

possible by the use of tunnel-diode discriminators with negligible slewing.[8] A typical discriminator curve is shown in Fig. 11.

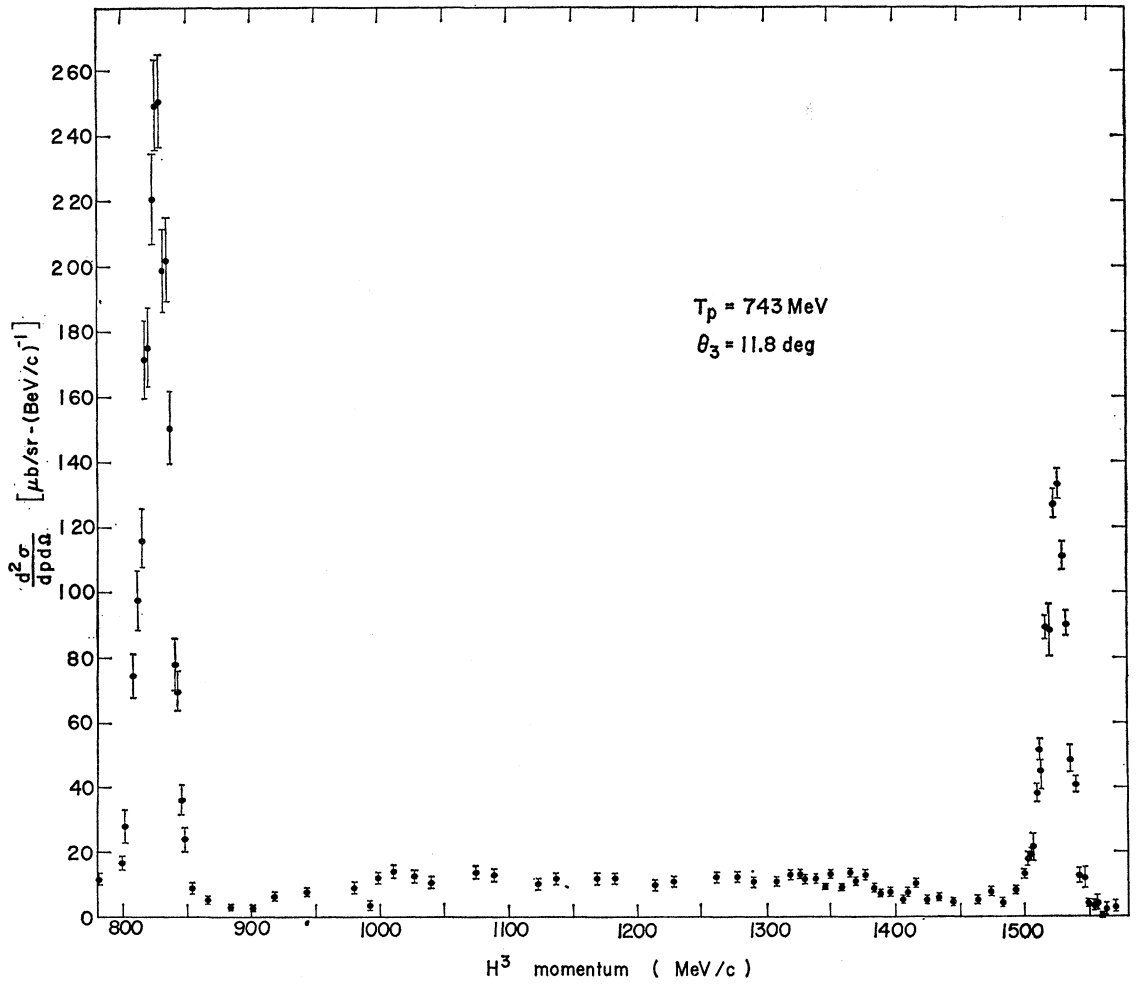

FIG. 15. Measured H^3 momentum spectrum for $\theta=11.8$ deg.

[8] A. E. Bjerke, Q. A. Kerns, and T. A. Nunamaker, Lawrence Radiation Laboratory Report UCRL-9838, 1961 (unpublished).

VII. MEASUREMENTS OF MOMENTUM SPECTRA

The actual data-taking consisted of measuring the yield of He^3 or H^3 of a particular momentum using the SEM as a monitor of the incident beam. Each run took about 30 min, and then a new momentum setting was made. Generally, the spectrum was taken in order, but occasionally points would be repeated at random. No significant difference was ever observed. Background measurements were performed by replacing the D_2 gas with H_2 gas of equal stopping power at about six momenta and were found to be less than 1% of the maximum rate. At the reduced energies measured in the first run the larger incident-beam size resulted in production of He^3 in the walls of the target vessel, and backgrounds ran as high as about 30% of the peak rate. A smooth slow variation of the background with He^3 or H^3 momentum was always observed with H_2 gas in the target, and we draw a smooth curve through these points to obtain the background at intermediate momenta.

Occasionally accidentals were taken by delaying S_1 one rf period. None were ever found, but we checked by taking some data with the proton beam reduced in intensity by a factor of two to four. These measurements always agreed well with the data taken at full beam intensity.

VIII. CORRECTIONS AND THE CALCULATION OF CROSS SECTIONS

Two basic corrections must be applied to the raw data to obtain differential cross sections. The first is the "momentum acceptance" correction. This occurs because our yields are measured per unit $\Delta p/p$ rather than per unit Δp. The second correction comes about because of the energy loss of the particles in traveling from the center of the target to the magnetic analyzer, and consists of two parts. Firstly, we must compute the momentum at production, p_0, for each momentum setting, p_s, of the bending magnets. That is, we have $p_0=p_s+\langle dp/dR\rangle_{\mathrm{av}}\Delta R$, where $\langle dp/dR\rangle_{\mathrm{av}}$ is a suitable average of $(1/\beta)(dE/dx)$ and ΔR is the thickness of material in g/cm² between the D_2 target and the bending magnets. Secondly, for particles in a given momentum interval Δp_0 at production there is a decrease in the flux per unit momentum interval by the factor $(dp/dR)_0/(dp/dR)_s$ due to the energy loss. These corrections are included in the formula for the cross section

$$\text{counts/monitor}=\left(\frac{\text{protons}}{\text{monitor}}\right)(\rho lN/A)\left(\frac{d^2\sigma}{dpd\Omega}\right)_0 \times(\Delta\Omega)\left(\frac{\Delta p}{p}\right)_s p_s\frac{(dp/dR)_0}{(dp/dR)_s},$$

where ρl is the effective surface density of deuterium in g/cm², N is Avogadro's number, A is the atomic weight of deuterium, and $d^2\sigma/dpd\Omega$ is the cross section per unit solid angle and unit momentum interval.

The only other correction is particle loss due to multiple scattering. This correction is negligible for the H^3 data and for the He^3 data above 1300 MeV/c. It increases to a 7% correction for the second run and a 1% correction for the third run at 1100 MeV/c.

The corrected He^3 data at 11.8, 13.5, and 15.7 deg and the H^3 data at 11.8 deg are shown in Figs. 12, 13, 14, and 15, respectively.

ACKNOWLEDGMENTS

We wish to acknowledge the generous assistance of R. B. Bacastow, R. L. Beck, P. B. Beilin, G. M. Bingham, J. B. Czirr, D. Jenkins, H. W. Kruger, R. R. Larsen, T. Maung, M. Pripstein, H. R. Rugge, R. E. Shafer, W. Tivol, and O. Vik who helped to set up the equipment and take data. We are grateful to Edwin F. McLaughlin and William L. Pope and the hydrogen target crew for design, testing, and installation of the high-pressure gas targets. Finally, we wish to thank James Vale and the entire cyclotron crew for capable and reliable operation of the cyclotron.